Cotranscriptional histone H2B monoubiquitylation is tightly coupled with RNA polymerase II elongation rate

Gilad Fuchs,[1,4] Dror Hollander,[2,4] Yoav Voichek,[3] Gil Ast,[2] and Moshe Oren[1]

[1]Department of Molecular Cell Biology, Weizmann Institute of Science, Rehovot 76100, Israel; [2]Department of Human Molecular Genetics and Biochemistry, Sackler Faculty of Medicine, Tel-Aviv University, Ramat Aviv 69978, Israel; [3]Department of Molecular Genetics, Weizmann Institute of Science, Rehovot 76100, Israel

Various histone modifications decorate nucleosomes within transcribed genes. Among these, monoubiquitylation of histone H2B (H2Bub1) and methylation of histone H3 on lysines 36 (H3K36me2/3) and 79 (H3K79me2/3) correlate positively with gene expression. By measuring the progression of the transcriptional machinery along genes within live cells, we now report that H2B monoubiquitylation occurs cotranscriptionally and accurately reflects the advance of RNA polymerase II (Pol II). In contrast, H3K36me3 and H3K79me2 are less dynamic and represent Pol II movement less faithfully. High-resolution ChIP-seq reveals that H2Bub1 levels are selectively reduced at exons and decrease in an exon-dependent stepwise manner toward the 3' end of genes. Exonic depletion of H2Bub1 in gene bodies is highly correlated with Pol II pausing at exons, suggesting elongation rate changes associated with intron–exon structure. In support of this notion, H2Bub1 levels were found to be significantly correlated with transcription elongation rates measured in various cell lines. Overall, our data shed light on the organization of H2Bub1 within transcribed genes and single out H2Bub1 as a reliable marker for ongoing transcription elongation.

[Supplemental material is available for this article.]

Histones undergo numerous post-translational modifications such as methylation, acetylation, phosphorylation, SUMOylation, and ubiquitylation, which occur primarily within histone tails and play multiple roles in regulating gene expression, chromatin dynamics, and DNA repair (Berger 2007; Kouzarides 2007; Weake and Workman 2008; Campos and Reinberg 2009; Zhou et al. 2011; Patel and Wang 2013). The best-studied examples of histone ubiquitylation are the monoubiquitylation of histone H2B on lysine 123 in yeast or lysine 120 in mammals (H2BK120ub1, abbreviated here as H2Bub1), and the monoubiquitylation of histone H2A on lysine 119. H2B can undergo ubiquitylation also on Lys34 (Wu et al. 2011). H2Bub1 is carried out by the yeast E3 ubiquitin ligase Bre1 (Hwang et al. 2003; Wood et al. 2003) and the orthologous heteromeric hBre1 (RNF20)/RNF40 mammalian complex (Kim et al. 2005; Zhu et al. 2005), while UBE2A and UBE2B are the corresponding E2 ubiquitin-conjugating enzymes (Kim et al. 2009).

H2Bub1 regulates multiple molecular processes such as transcription initiation and elongation (Davie and Murphy 1990; Henry et al. 2003; Pavri et al. 2006; Weinberger et al. 2012), DNA damage response (Chernikova et al. 2010; Kari et al. 2011; Moyal et al. 2011; Nakamura et al. 2011), DNA replication (Trujillo and Osley 2012), nucleosome positioning (Batta et al. 2011), and RNA processing and export (Pirngruber et al. 2009; Jung et al. 2012; Moehle et al. 2012; Vitaliano-Prunier et al. 2012; Herissant et al. 2014; Long et al. 2014). Aberrant H2Bub1 levels can affect development (Wright et al. 2011), apoptosis (Walter et al. 2010), stem cell differentiation (Buszczak et al. 2009; Fuchs et al. 2012; Karpiuk et al. 2012), viral infection outcome (Sarkari et al. 2009; Fonseca et al. 2012), and cell cycle progression (Hwang and Madhani 2009)

and can promote cancer (Shema et al. 2008; Blank et al. 2012; Johnsen 2012; Fuchs and Oren 2014). Several mechanisms have been proposed to underlie the ability of H2Bub1 to exert those diverse effects, including impact on higher-order chromatin organization (Fierz et al. 2011), altered nucleosome stability (Chandrasekharan et al. 2009), regulation of H2A-H2B dimer displacement (Pavri et al. 2006), and modulation of the recruitment of specific factors to chromatin (Shema-Yaacoby et al. 2013).

H2Bub1 ubiquitylation has been particularly linked with transcription regulation (for review, see Sen and Bhaumik 2013 and Fuchs and Oren 2014). Surprisingly, although H2Bub1 is associated preferentially with transcribed genes and its levels correlate positively with their expression rates (Minsky et al. 2008), transient knockdown of RNF20 affects only a relatively small fraction of the transcriptome (Shema et al. 2008). Other studies showed that while affecting only marginally steady-state transcription, H2Bub1 depletion has a more pronounced impact on inducible transcriptional programs triggered in response to various cues (Fuchs et al. 2012; Karpiuk et al. 2012; Weiner et al. 2012). Moreover, H2Bub1 is preferentially required for transcriptional induction of relatively long genes in response to retinoic acid (Fuchs et al. 2012), in agreement with an in vitro study implicating a positive role for H2Bub1 in transcription elongation (Pavri et al. 2006).

Chromatin immunoprecipitation experiments coupled with high-throughput sequencing (ChIP-seq), using H2Bub1-specific antibodies, revealed a nonrandom distribution of H2Bub1 within active gene bodies. While one study reported that H2Bub1 is significantly reduced following the first internal exon (Huff et al. 2010),

another study concluded that H2Bub1 is selectively enriched at exon–intron borders and proposed that this enrichment regulates the splicing of a subset of exons (Jung et al. 2012).

In addition to H2Bub1, the gene body of active genes is mostly decorated with histone H3 trimethylation on lysine 36 (H3K36me3) and with di- and trimethylation on lysine 79 (H3K79me2/3) (Barski et al. 2007; Wang et al. 2008; Huff et al. 2010). Moreover, H2Bub1 is proposed to stimulate H3K79me2/3 by histone crosstalk (Briggs et al. 2002; Ng et al. 2002; Lee et al. 2007). While the kinetic properties of H3K36me3 during transcription elongation have been studied (Wada et al. 2009; de Almeida et al. 2011), a comparative kinetic analysis of all three chromatin marks is still lacking.

Here we combine high-resolution ChIP-seq analysis of H2Bub1 and in vivo kinetic monitoring of transcription machinery progress to show that H2B is rapidly and reversibly mono-ubiquitylated cotranscriptionally during transcription elongation, while H3K36me3 and H3K79me2 are less dynamic and do not represent active transcription in a similar temporal resolution and accuracy as H2Bub1. The dynamic nature of H2Bub1 is reflected by its unique distribution within transcribed gene bodies. We further find that H2Bub1 is enriched in introns and selectively reduced in exons, and that H2Bub1 levels decrease toward the 3′ end of genes. Exonic H2Bub1 reduction correlates with accumulation of RNA polymerase II (Pol II), suggesting that H2Bub1 levels within gene bodies reflect changes in Pol II elongation rates that are probably associated with cotranscriptional splicing. In support of this notion, we find a significant correlation between H2Bub1 levels and experimentally measured transcription elongation rates. These results further elucidate the role of histone modifications within gene bodies and highlight H2Bub1's unique dynamic relationship with transcription elongation as compared to H3K36me3 and H3K79me2. Specifically, although H3K36me3 and H3K79me2 are positively correlated with transcription, our results suggest that they may not have an inherent role in the dynamic transcriptional elongation process. In contrast, the cotranscriptional ubiquitylation of histone H2B suggests that it may be more intimately involved in ongoing nucleosome turnover in the wake of Pol II.

Results

H2Bub1 is enriched in transcribed regions but depleted in exons, with stepwise drops between introns

To investigate in detail the genomic distribution of H2Bub1, ChIP-seq analysis of NTera2 (NT2) human embryonic carcinoma cells was performed with antibodies against H2Bub1 and non-modified H2B. In agreement with earlier findings (Minsky et al. 2008; Shema et al. 2008), we found that H2Bub1 is ubiquitously localized within gene bodies and depleted upstream of the transcription start sites (TSSs) (Supplemental Fig. S1A). Moreover, the levels of H2Bub1 as well as the relative levels of H2Bub1 normalized to H2B (H2Bub1/H2B) increase from the TSS into the 5′ part of the transcribed region and then gradually decrease toward the 3′ end (Fig. 1A; Supplemental Fig. S1A). In addition, a clear correlation between H2Bub1/H2B ratio and gene expression level was observed (Fig. 1A). In order to better characterize the distribution of H2Bub1 within genes, the H2Bub1/H2B ratios in various elements of all genes were determined and then compared to their expected levels if one corrects for each element's genomic size (Fig. 1B; Methods). As can be seen in Figure 1B, H2Bub1/H2B is significantly enriched in introns (χ^2 test, P-value $< 10^{-6}$) and depleted in promoters (P-value $< 10^{-6}$), 5′ UTRs (P-value = 0.03),

exons (P-value = 0.007), and translation stop codon regions (P-value $< 10^{-6}$).

Given the strong relative enrichment of H2Bub1 within introns and in the 5′ parts of genes, we compared the average H2Bub1/H2B ratios in the first three introns of all expressed genes (Fig. 1C). Surprisingly, although overall H2Bub1/H2B values decrease gradually toward the 3′ end of genes (Fig. 1A) and between introns (Fig. 1C), they remain relatively steady throughout a given intron, even though average introns are ~4000 bp long and much larger than the average exon, which is only 147 bp long (Gelfman et al. 2012). Notably, H2Bub1/H2B ratios in the first intron were higher in longer introns (Supplemental Fig. S1B). Given the steady H2Bub1/H2B values within introns and the overall decrease of H2Bub1/H2B along genes, we speculated that H2Bub1 decreases specifically at intron–exon borders. We therefore analyzed relative H2Bub1 levels within the first three exons of all expressed genes and the 250 bp surrounding them; alternative exons were omitted from the analysis. Exons bind nucleosomes preferentially when compared to introns (Schwartz et al. 2009; Tilgner et al. 2009), but normalization of the H2Bub1 signal to that of H2B cancels any exonic chromatin positioning bias. As expected from the total increase of H2Bub1/H2B near the 5′ end of genes, the relative H2Bub1 signal increased after the first exon, relative to the promoter region preceding it (Supplemental Fig. S1C). In contrast, for both the second and third exons, the average normalized H2Bub1 signal was lower after the exon than before it (Supplemental Fig. S1C). In addition, a marked reduction in H2Bub1 was indeed observed within the second and third exons compared with their flanking introns (Supplemental Fig. S1C). Thus, with the exception of the first exon, H2Bub1 levels are relatively low in exons and drop in a stepwise manner after exons.

To examine whether the drop in H2Bub1 between consecutive introns and its relative reduction in exons are not merely the result of sequence content biases between exons and introns, we compared the H2Bub1 pattern in functional (spliced) exons of expressed genes to that of two other data sets. The first data set includes 36,135 exonic composition regions (ECRs), exon-sized regions within introns of expressed genes possessing sequence content similar to that of exons but not actually serving as exons (Spies et al. 2009). The second includes 134,935 pseudo exons, defined as intronic regions of expressed genes with a length distribution similar to that of exons, flanked by relatively strong splicing signals (Ke et al. 2011). The results of this analysis (Fig. 1D) clearly indicate that the H2Bub1 signal drops between consecutive introns and that the reduction within exons is specific to functional exons, as it is not exhibited at ECRs or pseudo exons. Furthermore, similar results were observed in HCT116 cells (Supplemental Fig. S1D; data from Zhang et al. 2013), confirming that this is a global phenomenon. Given the reduced exonic H2Bub1 levels as well as the signal drops between consecutive introns, we speculated that the overall reduction in H2Bub1 toward the 3′ end of genes would be more pronounced in genes with a higher number of exons. Indeed, as shown in Supplemental Figure S1E, this was found to be the case. To ensure that this is not due to gene length rather than to number of exons, the first 10 kb of all expressed multiexonic genes longer than 20 kb was examined (Fig. 1E). Again, H2Bub1 decreased more strongly in genes with more exons within their first 10 kb. Altogether, we find that H2Bub1 levels in expressed genes decrease toward their 3′ end in a manner that is positively correlated with the presence of exons, while the exons themselves exhibit low H2Bub1 levels compared to their flanking introns (for specific examples, see Fig. 1F).
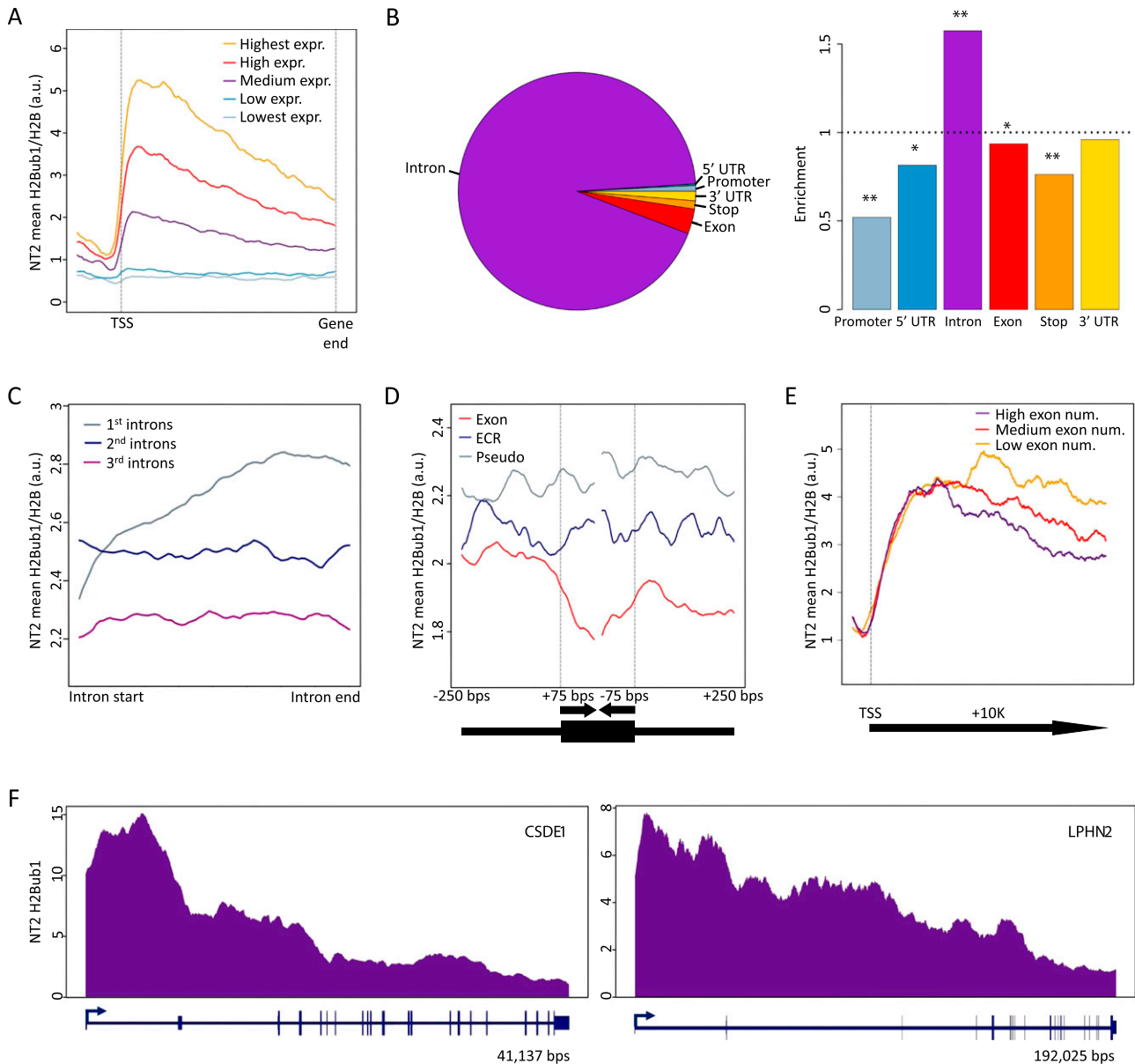
Figure 1. H2Bub1 is preferentially localized in transcribed regions and is reduced in exons. (*A*) Mean H2Bub1/H2B ratios—deduced from ChIP-seq in NT2 cells (*y*-axis)—of genes grouped according to their expression level. Gene bodies were scaled to fit in 100 equally sized bins from their transcription start site (TSS) to their 3′ end (*x*-axis). A moving average of five was applied. (*B, left*) Pie chart depicting the fraction of H2Bub1/H2B peaks (Methods) in each of six gene segments ([UTR] untranslated region; [stop] translation stop codon). (*Right*) Relative enrichment of H2Bub1/H2B peaks across the gene segments corrected for their genomic size. (*) χ^2 test *P*-value < 0.05; (**) *P*-value $< 10^{-6}$. (*C*) Mean H2Bub1/H2B ratio in NT2 cells (*y*-axis) of first, second, and third introns of expressed genes (gray, blue, and purple, respectively). Introns were scaled to fit in 100 equally sized bins (*x*-axis). A moving average of 20 was applied. (*D*) Mean H2Bub1/H2B ratio in NT2 cells (*y*-axis) of internal exons (exon), exonic composition regions (ECRs), and pseudo exons (pseudo; red, blue and gray, respectively) in expressed genes. Seventy-five base pairs from each region end and the 250 bp adjacent to them were plotted (*x*-axis). A moving average of 20 was applied. (*E*) Mean H2Bub1/H2B ratio in NT2 cells (*y*-axis) of multiexonic expressed genes longer than 20 kb, grouped according to the number of exons in their first 10 kb; 1.1 kb upstream of the TSS to 10 kb downstream from it was plotted (*x*-axis). A moving average of 700 was applied. (*F*) Distribution of H2Bub1 ChIP-seq reads along the *CSDE1* and *LPHN2* genes (*y*-axis). Gene architecture is shown for each gene from start to end (*x*-axis), with thick lines corresponding to exons and thin lines corresponding to introns. (a.u.) Arbitrary units.

Exonic H2Bub1 levels are independent of splicing

The observed correlation between H2Bub1 and transcription level, as well as the unique H2Bub1 distribution at exon–intron borders, raised the possibility that this might reflect either gene body Pol II dynamics (Braunschweig et al. 2013; Kornblihtt et al. 2013; Kwak et al. 2013) or an effect of splicing on H2Bub1 levels. To assess whether the low exonic H2Bub1 levels are dictated by the splicing program, we employed siRNA-mediated knockdown of the poly-pyrimidine tract–binding proteins PTBP1 (also known as PTB) and PTBP2 (also known as nPTB) in order to alter the inclusion level of specific alternative exons in HeLa cells. As reported (Llorian et al. 2010), knockdown of *PTBP1* and *PTBP2* resulted in significant exclusion of *OSBPL9* exon 9 and higher inclusion of *WNK1* exon
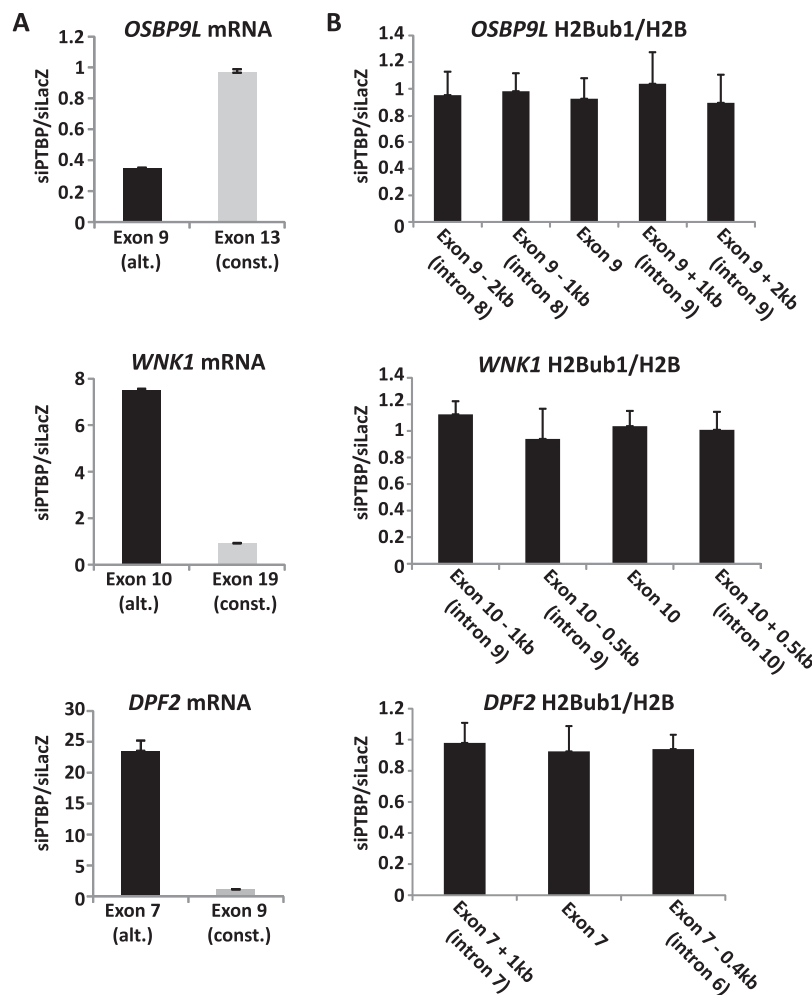
Figure 2. Exonic H2Bub1 levels are splicing independent. (*A*) HeLa cells were transfected with siRNA oligonucleotides (SMARTpool) directed against *PTBP1* and *PTBP2* (siPTPB) or against *lacZ* (siLacZ) as a control and 72 h later were analyzed by qRT-PCR with primers corresponding to the indicated exons. All values were normalized to *GAPDH* in the same sample and represent averages from duplicate qPCR reactions. Error bars, SD. Similar results were obtained in three independent experiments. (*B*) Cells were treated as in panel *A* and subjected to ChIP analysis with antibodies specific for H2B and H2Bub1. Immunoprecipitated DNA was quantified by qPCR with primers specific for the indicated regions. Bars indicate H2Bub1 ChIP readings normalized to H2B and represent averages from four experiments. H2Bub1/H2B ratios in siPTBP samples were normalized to siLacZ samples, which were defined as 1.0.

(H3K36me3 data from Blahnik et al. 2011), confirmed that H3K36me3 was markedly depleted in intronless genes, particularly highly expressed ones (Supplemental Fig. S2A). In contrast, H2Bub1 displayed a very different pattern and was only slightly higher in the intronless genes (Supplemental Fig. S2B), which are relatively short; this is consistent with the trend of the exon-dependent H2Bub1 decrease seen more strongly in longer genes (see Fig. 1).

Global H2Bub1 levels are tightly coupled with active transcriptional elongation

To further explore the relationship between H2Bub1 and transcription, the effect of the reversible p-TEFb inhibitor 5,6-Dichloro-1-β-D-ribofuranosylbenzimidazole (DRB) on global H2Bub1 levels was examined (Fig. 3). Since DRB specifically inhibits the transition from transcriptional initiation to active elongation, Pol II molecules already engaged in active elongation are not inhibited by it (Singh and Padgett 2009). As a result, DRB has a cumulative inhibitory impact on transcriptional output during early times of treatment. Indeed, exposure of HeLa cells to DRB decreased global H2Bub1 levels in a time-dependent manner (Fig. 3A). In contrast, H3K36me3 and H3K79me2 were un-affected within this relatively short time frame (Fig. 3A). Furthermore, restoration of transcription upon removal of DRB after 3 h resulted in a relatively rapid recovery of H2Bub1, while H3K36me3 and H3K79m2 did not change (Fig. 3B). Hence, global H2Bub1 levels mirror active Pol II transcription elongation more closely than H3K36me3 and H3K79me2.

10 and *DPF2* exon 7 (Fig. 2A). Adjacent constitutive exons from the same genes showed no significant change in inclusion level upon siRNA treatment, confirming that these exons were affected specifically (Fig. 2A). Remarkably, despite the substantial changes in specific exon inclusion, no significant change in relative H2Bub1 levels within the affected exons or their surrounding introns was observed (Fig. 2B). Hence, exonic H2Bub1 patterns are not dictated by the selective activity of the splicing machinery.

H3K36me3 is localized in the transcribed region of genes, in positive correlation with their expression levels (Barski et al. 2007; Wang et al. 2008), and preferentially marks exons (Kolasinska-Zwierz et al. 2009; Schwartz et al. 2009; Tilgner et al. 2009). H3K36me3 levels are greatly enhanced by splicing, and intronless genes exhibit significantly less H3K36me3 relative to intron-containing genes (de Almeida et al. 2011). Indeed, comparison of ChIP-seq signals in NT2 cells across intronless versus intron-containing genes up to 5 kb long, divided into three gene expression bins

H2B is monoubiquitylated cotranscriptionally

To obtain further insights into the coupling between H2Bub1 and active transcription, the dynamics of monoubiquitylation during real-time progression of the transcription machinery was monitored. Previously, DRB was employed in order to track the progress of Pol II by measuring the emergence of pre-mRNA from different regions of long genes (Singh and Padgett 2009). To track the progress of H2Bub1 during transcription elongation, we employed a similar approach in combination with H2Bub1 ChIP. HeLa cells were treated for 3 h with DRB and harvested at 10- or 15-min intervals after DRB removal to measure pre-mRNA and H2Bub1 levels. As can be seen from the pre-mRNA analysis in Figure 3C, transcription of a proximal region located 1 kb downstream from the TSS of the *TTC17* gene resumed fully within 10 min after DRB removal. In contrast, transcription of a distal region of the same gene, located 92 kb downstream from the TSS, recovered only 30–40 min after drug release, consistent with the genomic distance
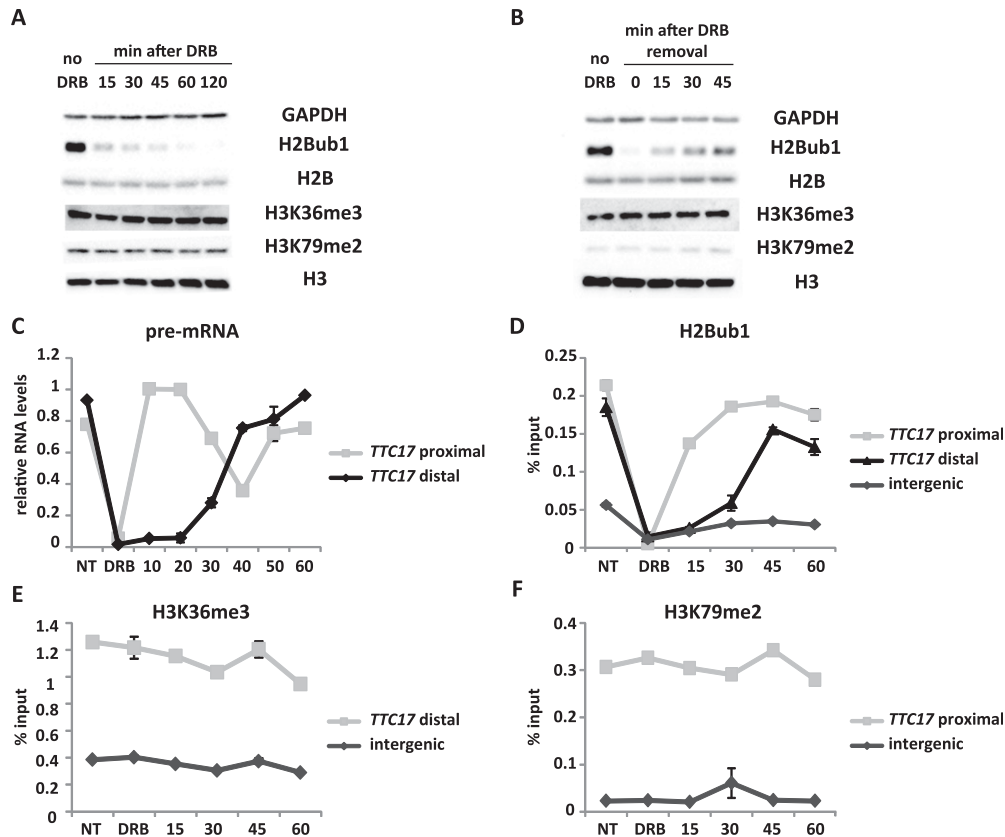
Figure 3. H2B is monoubiquitylated cotranscriptionally. (*A*) HeLa cells were treated with 100 μM DRB for the indicated times, and cell extracts were subjected to Western blot analysis with the indicated antibodies. (*B*) HeLa cells were either not treated (no DRB) or treated with 100 μM DRB for 3 h, and harvested at the indicated time points after DRB removal. Cell extracts were subjected to Western blot analysis with the indicated antibodies. (*C*) qRT-PCR analysis of *TTC17* pre-mRNA in HeLa cells in proximal (1 kb downstream from the TSS) and distal (92 kb downstream from the TSS) regions of the gene, following 3 h of 100 μM DRB treatment (DRB) and at the indicated time points after DRB removal. All values were normalized to 16S rRNA in the same sample. (*D–F*) Treatment as in *C*, but cells were subjected to ChIP analysis with antibodies against H2Bub1 (*D*), H3K36me3 (*E*), and H3K79me2 (*F*). Bars indicate ChIP readings normalized to input in the same treatment and represent averages from duplicate qPCR reactions; error bars, SD. Similar results were obtained in four independent experiments.

between the two regions. Notably, H2Bub1 levels at the same sites mirrored almost precisely the accumulation of the pre-mRNA (Fig. 3D). Similar results were observed for additional genes, regardless of whether H2Bub1 was normalized to input or to nonmodified H2B (Supplemental Fig. S3A–C; data not shown), as well as in NT2 cells (Supplemental Fig. S3D). Consistent with the coupling between H2Bub1 and Pol II progression, slowing down the elongation rate by placing the cells at 32°C resulted in a similar reduction in the spreading kinetics of H2Bub1 (Supplemental Fig. S4A,B). Hence, H2Bub1 is highly coupled to the transcription elongation process, concurring with the progress of Pol II.

H3K36me3 is widely regarded as a mark of active elongation. However, most of the studies examine H3K36me3 levels under steady-state conditions, and the few studies that did test the dynamic behavior of H3K36me3 reached contradicting conclusions (Edmunds et al. 2008; Wada et al. 2009; de Almeida et al. 2011; Le Martelot et al. 2012; Yu et al. 2013). Thus, we examined the dynamics of H3K36me3 during transcription elongation using the same assay as above. In agreement with the DRB nonresponsiveness of global H3K36me3 during relatively short time scales (Fig. 3A,B), the distribution of H3K36me3 on *TTC17* and additional genes barely changed after 3 h of DRB treatment or within 1 h after DRB removal (Fig. 3E; data not shown).

Similarly to H3K36me3, H3K79me2/3 is also positively correlated with gene expression and is employed as a marker of active elongation (Guttman et al. 2009). Studies in yeast and mammals suggested that H2Bub1 is a prerequisite for H3K79me2/3 (Briggs et al. 2002; Ng et al. 2002; Sun and Allis 2002). To further explore the coupling between H2Bub1 and H3K79me2/3 and assess the dynamic behavior of H3K79me2/3 during transcription elongation, H3K79me2 ChIP was performed as above. As seen in Figure 3F, unlike the dynamic nature of H2Bub1, H3K79me2 was much more stable and not influenced significantly by DRB treatment or its removal. Overall, these findings imply that elongation-related H3 methylations are much more persistent and less dynamic than H2Bub1. Thus, while H2Bub1 reflects the transcription elongation status at a minute-scale resolution, those other histone modifications do not.

Surprisingly, in addition to its dynamic behavior within transcribed gene bodies, H2Bub1 displayed a similar behavior also at random intergenic regions located at least 25 kb away from the nearest gene (Supplemental Fig. S5), decreasing significantly after 3 h of DRB treatment and increasing again within 15 min after DRB removal. It is likely that the presence of H2Bub1 at intergenic regions reflects pervasive transcription at those regions, implying that intergenic transcription is regulated in a similar manner to

that of typical Pol II–dependent genes. In addition, in some genes H2Bub1 increased mildly at distal regions of long genes within minutes after DRB removal, well before the expected arrival of Pol II to these regions (Fig. 3D; Supplemental Figs. S3B,C), suggesting that pervasive transcription might initiate anywhere in the genome, including within gene bodies of active genes.

Gene body H2Bub1 dynamics in response to EGF mirror transcriptional induction

To study the dynamic behavior of H2Bub1, H3K36me3, and H3K79me2 in a biologically relevant context, we examined the relationship between transcription and these three modifications in HeLa cells exposed to epidermal growth factor (EGF). Levels of pre-mRNA, H2Bub1, H3K36me3, and H3K79me2 in the gene body of the early response genes *EGR1* and *JUN* (Amit et al. 2007) were monitored at different time points. In agreement with the dynamic nature of H2Bub1 in response to DRB, EGF caused a transient increase in H2Bub1 within the transcribed region of *EGR1*, mirroring a transient surge in *EGR1* pre-mRNA 30 min after treatment (Fig. 4A,B). Subsequently, both *EGR1* pre-mRNA and H2Bub1 rapidly returned to basal levels. In contrast, consistent with an earlier report (Edmunds et al. 2008), H3K36me3 increased within 30 min of EGF treatment but remained high also at later times, when transcription had already been turned off (Fig. 4B, 60 and 120 min). H3K79me2 remained unchanged throughout that period (Fig. 4B). Furthermore, whereas both *JUN* pre-mRNA and H2Bub1 increased markedly 30 min after EGF treatment and

remained high at 120 min, neither H3K36me3 nor H3K79me2 exhibited a comparable increase (Fig. 4C,D). Thus, H2Bub1 levels reflect transient transcriptional induction more accurately than H3K36me3 and H3K79me2.

H2Bub1 levels are significantly correlated with genome-wide elongation rates in multiple cell lines

Given the high concordance between H2Bub1 and transcription elongation, we wished to examine more directly the correlation between Pol II elongation rates and H2Bub1 levels at a genome-wide scale. To that end, we employed the recently described 4sUDRB-seq method (Fuchs et al. 2014). Specifically, we examined the correlation between elongation rates determined by 4sUDRB-seq in epithelial HeLa cells and H2Bub1 levels determined by H2Bub1 ChIP-seq in epithelial HCT116 cells as well as in NT2 cells. As seen in Figure 5A, a significant correlation was found between elongation rates and genome-wide H2Bub1 occupancy in both cell lines. H2Bub1 was significantly higher in genes of the fast elongation rate quartile of both HCT116 and NT2 cells (Student's *t*-test, *P*-values = 6.45×10^{-16} and 1.23×10^{-12}, respectively), relative to the slow elongation rate quartile (Fig. 5B). Of note, H2Bub1 levels in both HCT116 and NT2 cells correlated better with HeLa cell transcription elongation rates (Pearson, $R = 0.33$ and $R = 0.3$, respectively) than with HeLa gene expression levels (Pearson, $R = 0.22$ and $R = 0.18$, respectively). Likewise, the correlation between H2Bub1 levels in HCT116 and NT2 cells and transcription initiation rates in HeLa cells, mea-
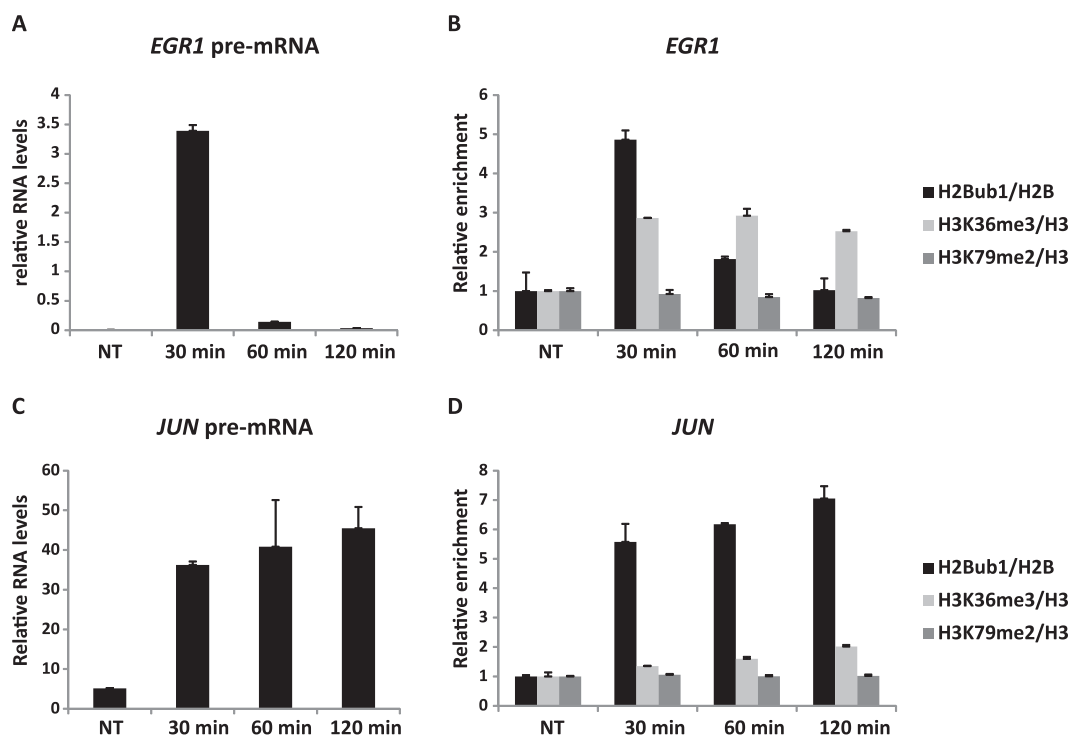

Figure 4. Gene body H2Bub1 dynamics in response to EGF mirror transcription patterns. (*A*) HeLa cells were serum starved for 16 h and then stimulated with EGF (20 ng/mL) for the indicated periods. *EGR1* pre-mRNA was quantified by qRT-PCR. All values were normalized to *GAPDH* pre-mRNA in the same sample. Bars indicate averages from duplicate qPCR reactions; error bars, SD. Similar data were obtained in three independent experiments. (*B*) Treatment as in *A*, but cells were subjected to ChIP analysis with antibodies against H2Bub1, H3K36me3, and H3K79me2. Immunoprecipitated DNA was quantified by qPCR with primers specific for the 5′-transcribed region of *EGR1*. Bars indicate ChIP readings normalized to H2B or H3 in the same treatment and represent averages from duplicate qPCR reactions; error bars, SD. Similar results were obtained in three independent experiments. (*C*) As in *A*, but *JUN* pre-mRNA was measured. (*D*) As in *B*, but primers specific for the 3′ transcribed region of *JUN* were used.
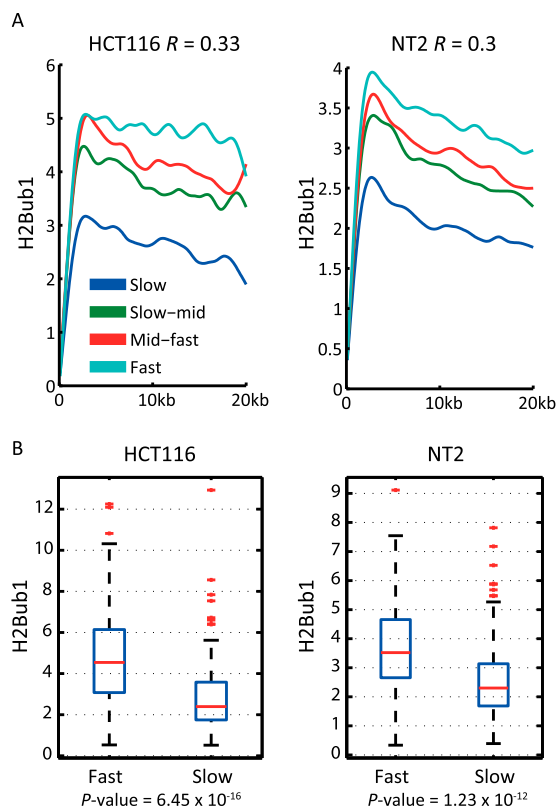
Figure 5. Genome-wide correlation between H2Bub1 levels and elongation rates. (*A*) Genome-wide transcription elongation rates were determined in HeLa cells by DRB4sU-seq (Fuchs et al. 2014) . Genes longer than 25 kb were ranked according to elongation rate and binned in four equally sized groups (from fastest to slowest: turquoise, red, green, and blue). Mean H2Bub1 ChIP-seq values for the first 20 kb downstream from the TSS in either HCT116 colorectal cancer cells (*left*) or NT2 cells (*right*) were plotted for each group. Data were smoothed using cubic spline with parameter 0.001. *R* denotes the Pearson correlation coefficient between elongation rates and H2Bub1 occupancy. (*B*) Mean H2Bub1 levels within genes included in the top 25% ("Fast") or the bottom 25% ("Slow") elongation rate gene groups, defined as in *A*. Mean H2Bub1 levels are significantly higher in Fast genes (Student's *t*-test; *P*-values = 6.45×10^{-16} and 1.23×10^{-12} for HCT116 and NT2 cells, respectively).

sured by 4sUDRB-seq (Fuchs et al. 2014), was also weaker (Pearson, $R = 0.19$ and $R = 0.17$, respectively).

A method essentially similar to 4sUDRB-seq (BruDRB-seq) has recently been employed to determine elongation rates in five different cell lines (Veloso et al. 2014). Of note, elongation rates of individual genes are well conserved across cell lines (Veloso et al. 2014). Reassuringly, we found that H2Bub1 levels correlate significantly with elongation rates in all these lines as well (Supplemental Fig. S6A).

Exons with low H2Bub1 levels are characterized by high Pol II occupancy

The significant correlation between H2Bub1 and transcription elongation rates raised the possibility that the uneven distribution of H2Bub1 within exons and at intron–exon borders might relate to differential Pol II dynamics in those regions. Pol II has been shown to pause or slow down upstream of exons, presumably underlying a regulatory effect of elongation rate on cotranscriptional splicing (de la Mata et al. 2003; Schor et al. 2009, 2013; Ip et al. 2011; Luco et al. 2011; Kwak et al. 2013). We therefore ex-

amined the ChIP-seq signal of transcriptionally engaged elongating (Ser2P) Pol II in HCT116 cells (data from Maunakea et al. 2013) at exons of expressed genes and their surrounding intronic regions. To avoid bias due to promoter proximity, all first exons were omitted from the analysis. While exonic composition regions (ECRs) and pseudo exons exhibited no Ser2P-Pol II enrichment, we found that Ser2P-Pol II levels increase upstream of exon 5′ ends and decrease toward their 3′ ends (Fig. 6A). In agreement with previous findings (Kwak et al. 2013; Maunakea et al. 2013), this implies that a global reduction in Pol II elongation rate occurs specifically upstream of functional exons. To determine whether this is also associated with a corresponding H2Bub1 pattern, we next compared two exon groups differing in their H2Bub1 distribution (Fig. 6B): 6649 exons with markedly reduced H2Bub1 relative to their surroundings, defined by differential intron–exon H2Bub1 levels, and 5309 exons not displaying such H2Bub1 reduction (red and blue boxes, respectively). Notably, exons with reduced H2Bub1 levels exhibited greater Ser2P-Pol II occupancy at their 5′ ends compared with exons without local H2Bub1 reduction (Student's *t*-test, *P*-value $< 6 \times 10^{-16}$) (Fig. 6C), suggesting that reduced exonic H2Bub1 is coupled with reduced Pol II elongation rate. To better assess the correlation between H2Bub1 reduction and Pol II occupancy, we calculated the difference for both Ser2P-Pol II and H2Bub1 levels in exons relative to their flanking introns and observed a positive correlation between the extent of exonic H2Bub1 reduction and the degree of Ser2P-Pol II exonic enrichment (Fig. 6D). A similar correlation was also found upon analysis of ChIP-seq data (The ENCODE Project Consortium 2012) generated with a total Pol II antibody, which recognizes the large subunit, POLR2A (Supplemental Fig. S7). Thus, our results support the notion that H2Bub1 reduction is correlated with Pol II pausing rather than with Ser2 phosphorylation state. Together, our findings further support the relationship between Pol II kinetic changes and intron–exon structure and demonstrate that the distribution of H2Bub1 within active genes represents the corresponding Pol II changes in elongation rate.

Discussion

In this study, we provide insight into the unique distribution of H2Bub1 within gene bodies. We show that, in contrast to H3K36me3 and H3K79me2, H2Bub1 is regulated in a highly dynamic manner and is tightly coupled with local transcription elongation rates, which often vary between exons and introns. This is schematically depicted in Figure 7.

The differential distribution of H2Bub1 within gene bodies with regard to exon–intron architecture was addressed in two previous studies. Huff et al. (2010) showed that H2Bub1 levels decrease following the first internal exon, while Jung et al. (2012) reported that H2Bub1 is mainly enriched at exon borders. Our analysis of H2Bub1 distribution in NT2 and HCT116 cells agrees with the reported reduction in H2Bub1 after the first internal exon but extends this notion by showing that exons downstream from the first internal exon are associated with stepwise drops in H2Bub1. Indeed, genes with abundant exons exhibit a stronger reduction in H2Bub1 toward their 3′ end (Fig. 1E; Supplemental Fig. S1E). Furthermore, this unique H2Bub1 pattern is highly reflective of transcription elongation dynamics. In contrast, we could not fully recapitulate the accumulation of H2Bub1 at exon–intron borders reported by Jung et al. (2012). By normalizing the H2Bub1 signal for H2B occupancy, thus canceling differential chromatin positioning biases at exons compared to introns (Schwartz et al. 2009; Tilgner et al. 2009), we find that H2Bub1 is not
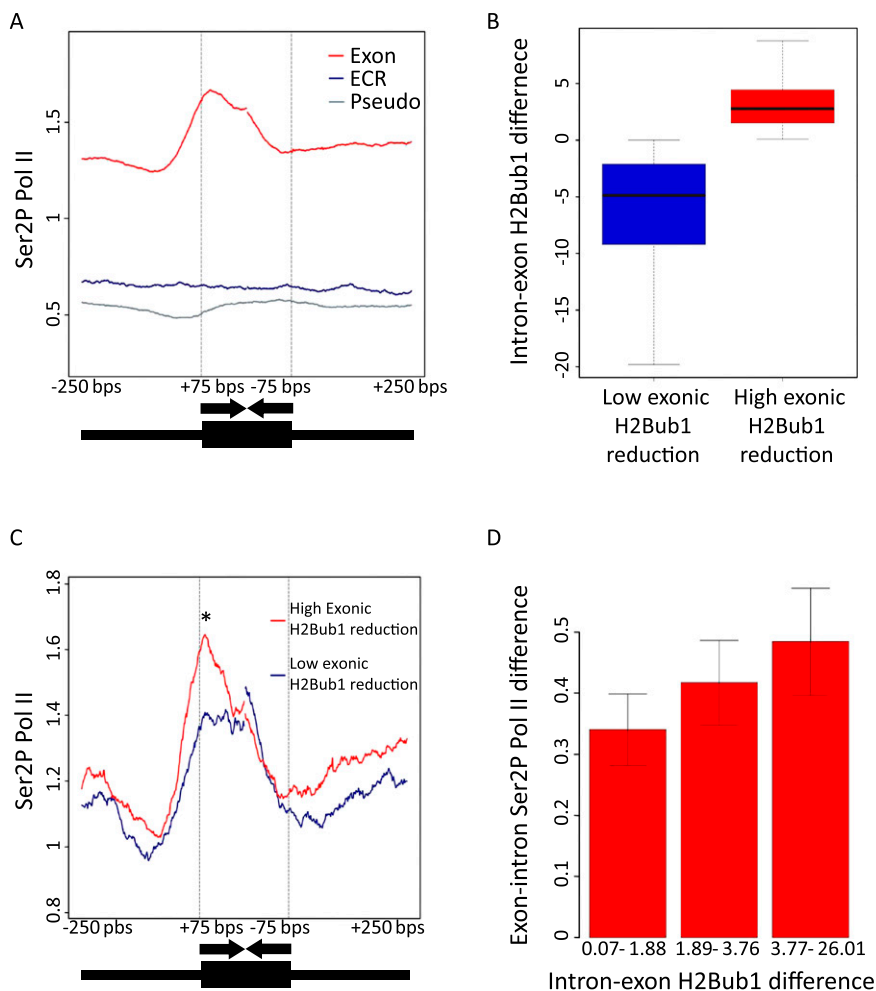
Figure 6. Exons with low H2Bub1 levels are characterized by high Ser2P-Pol II occupancy. (*A*) Mean Ser2P-Pol II ChIP-seq levels in HCT116 cells (*y*-axis) of internal exons (exon), exonic composition regions (ECR), and pseudo exons (pseudo; red, blue, and gray, respectively) in expressed genes. Seventy-five base pairs from each region end and the adjacent 250 bp were plotted (*x*-axis). (*B*) Box plot representing the distribution of intron–exon differential H2Bub1 values (intron–exon H2Bub1 difference), based on 75 bp of the exon and the first 250 bp of the adjacent intron, of exon groups in HCT116 cells without ($n = 5309$) and with ($n = 6649$) reduced H2Bub1 levels (blue and red, respectively). Thick black line indicates the median value of each group. Boxes enclose values between the first and third quartile. (*C*) Mean Ser2P-Pol II ChIP-seq levels in HCT116 cells (*y*-axis) of the same exon groups as in *B* 75 bp from each exon end and the adjacent 250 bp were plotted (*x*-axis). (*D*) Mean Ser2P-Pol II exonic enrichment (*y*-axis; denoted by mean exon–intron differential Ser2P-Pol II values) in HCT116 cells plotted against the intron–exon H2Bub1 differential (*x*-axis).

accumulated at exon–intron borders but rather is reduced in exons. We also note that Jung et al. (2012) examined H2Bub1 levels at 600-bp-long exonic regions aligned to both exon ends. However, the average human exon is only 147 bp long, and this has been conserved throughout evolution (Gelfman et al. 2012). Hence, we believe that monitoring the normalized H2Bub1 signal at 75-bp-long exonic regions aligned to both exon ends, as done here, provides a more accurate picture of the distribution of H2Bub1 within exons.

The observation that H2Bub1 is reduced in the majority of exons might imply that H2Bub1 is affected by the splicing process. However, altering the splicing pattern of specific exons by depletion of the alternative splicing factors PTBP1 and PTBP2 did not affect the level or distribution of H2Bub1 at these exons or their flanking introns. Thus, H2Bub1 levels are not determined by premRNA splicing. Like H2Bub1, the distribution of H3K36me3 is also

associated with exon–intron architecture (Kolasinska-Zwierz et al. 2009; Schwartz et al. 2009; Tilgner et al. 2009). In addition, H3K36me3 distribution has been shown to be determined by pre-mRNA splicing (Kim et al. 2011). In agreement, genome-wide H3K36me3 levels correlate with gene expression only in intron-containing genes (Supplemental Fig. S2; de Almeida et al. 2011), while H2Bub1 reflects transcriptional activity regardless of introns.

Interestingly, we observed a strong correlation between Ser2P-Pol accumulation at the 5′ ends of functional exons and H2Bub1 reduction at these sites. The negative relationship between H2Bub1 and Pol II accumulation, as well as the strong coupling between H2Bub1 and ongoing transcription elongation, suggest that H2Bub1 patterns are determined mainly by Pol II elongation kinetics. In other words, the low levels of H2Bub1 at exons may be a result of low elongation rates and transient arrest of Pol II at exons, which in some cases might result in dissociation of Pol II from the chromatin. Conceivably, the dependence could be in the opposite direction; namely, H2Bub1 levels might affect the elongation rate or processivity of Pol II rather than the other way round. However, since inhibition of Pol II elongation by DRB strongly affects global H2Bub1 levels (this study), whereas depletion of H2Bub1 alters the expression of only a minority of genes (Shema et al. 2008), we favor the option that the global pattern of H2Bub1 is dictated by Pol II elongation and not vice versa; whereas the opposite relationship—namely, regulation of transcription by H2Bub1—depends on different, gene-specific mechanisms that pertain only to a limited subset of genes. Similar to H2Bub1, we and others recently showed that H3K79me2 levels are also correlated with elongation rates (Fuchs et al. 2014; Jonkers et al. 2014; Veloso

et al. 2014). However, as shown here, H3K79 methylation is much more stable than H2Bub1. Hence, the crosstalk with transcriptional elongation is substantially more dynamic in the case of H2Bub1 than that of H3K79me2.

Intriguingly, following DRB treatment, H2Bub1 levels were significantly reduced at randomly chosen intergenic regions, including heterochromatic regions. Thus, phosphorylation of Pol II at both the intragenic and intergenic regions may be necessary for nonregulated pervasive transcription. In agreement with this notion, H2Bub1 was recently found to promote intergenic transcription within centromeres (Sadeghi et al. 2014). However, although we could detect H2Bub1 in these regions, we could not detect any corresponding RNA, leaving open the possibility that H2Bub1 is uncoupled from transcription in intergenic regions. In such case, low levels of H2Bub1 might be present throughout the chromatin in
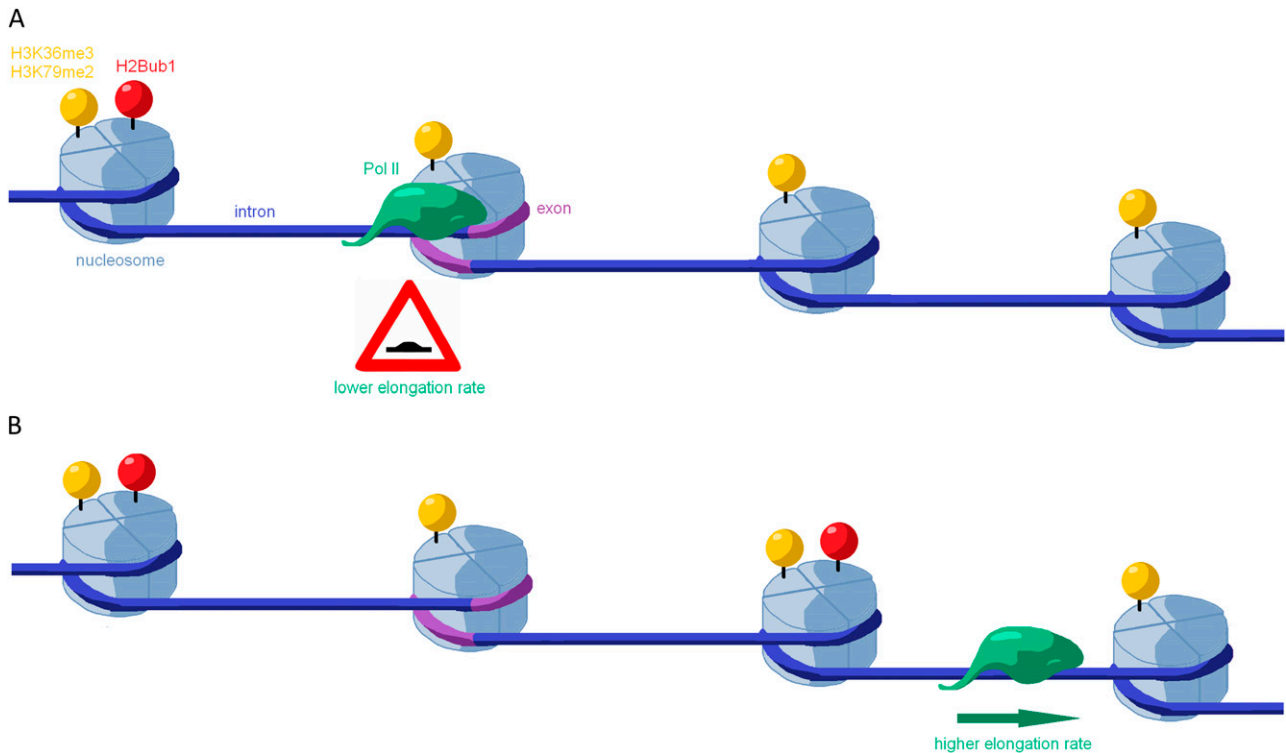
Figure 7. Model depicting the coupling between H2Bub1 distribution within gene bodies and Pol II elongation rate. H2Bub1 distribution is highly coupled to Pol II elongation within transcribed regions. While H3K36me3 and H3K79me2 do not mirror Pol II kinetics at this time resolution, H2B is monoubiquitylated as Pol II progresses along the gene (A to B). Furthermore, Pol II pausing or a slower elongation rate at exons compared to flanking introns is coupled with lower H2Bub1 levels.

order to keep it relatively open or to endow it with other specific structural features. Thus, the increase in H2Bub1 during differentiation of embryonic and adult stem cells (Fuchs et al. 2012; Karpiuk et al. 2012) may not necessarily be coupled with transcription but rather may have a global role in modulating chromatin structure as part of the differentiation program (Meshorer et al. 2006).

In sum, although H3K36me3 and H2Bub1 are both localized in gene bodies and their distribution is influenced by the presence of exons and introns, we find significant discordance between these two modifications. The highly dynamic spreading of H2Bub1 is consistent with former suggestions that H2B is monoubiquitylated transiently during the disassembly and reassembly of the nucleosome in the wake of Pol II (Pavri et al. 2006; Fleming et al. 2008). In contrast, the less dynamic behavior of H3 methylations may suggest that they do not have a direct role in transcription elongation. Rather, gene body H3 methylations may be involved in functions that do not demand a highly dynamic behavior, such as marking genes that were previously transcribed, suppressing histone exchange and cryptic transcription (Venkatesh et al. 2012), or affecting alternative splicing (Luco et al. 2010). Indeed, a recent study concluded that the presence of H3K36me2/3 in the coding regions of *Hox* genes occurs independently of productive transcriptional elongation (Miyazaki et al. 2013). Thus, we propose that H2Bub1 should be employed as the most reliable indicator of active transcriptional elongation.

Methods

Cell culture and transfection

All cells were maintained at 37°C. Ntera2/D1 cells were grown in RPMI (Biological Industries) supplemented with 10% heat-inactivated

fetal bovine serum (FBS, Hyclone), 2 mM L-glutamine, 1 mM sodium pyruvate, 0.1 mM nonessential amino acid, and penicillin–streptomycin antibiotics solution (all from Biological Industries). Human cervical carcinoma HeLa cells were grown in DMEM with 10% bovine serum supplemented with antibiotics. SMARTpool oligonucleotides for siRNA transfection were purchased from Dharmacon. Transfections were carried out with Dharmafect 1 reagent according to the manufacturer's protocol. All siRNA oligos were used at a final concentration of 25 nM.

RNA purification and quantitative RT-PCR

For quantitative reverse transcription (RT)-PCR analysis, total RNA was extracted with the miRNeasy kit's procedure (Qiagen). Two micrograms of each RNA sample was reverse transcribed with Moloney murine leukemia virus reverse transcriptase (Promega) and random hexamer primers (Applied Biosystems). Real-time PCR was done in a StepOne real-time PCR instrument (Applied Biosystems) with SYBR Green PCR supermix (Invitrogen). Primers used in this study are listed in Supplemental Table 1.

Antibodies

The following antibodies were used: anti-H2B (07-371, Millipore), anti-GAPDH (MAB374, Millipore), anti-H3 (ab1791, Abcam), anti-H3K36me3 (ab9050, Abcam), and anti-H3K79me2 (ab3594, Abcam). Anti-H2Bub1 is described in Minsky et al. (2008).

ChIP and high-throughput sequencing

Cells were fixed by adding one-tenth volume of an 11% formaldehyde solution directly to the medium, for 10 min at room

temperature. After fixation, cells were washed twice and harvested. To extract chromatin, cells were resuspended in 1 mL of cell lysis buffer (50 mM PIPES, 85 mM KCl, 0.5% NP-40); nuclei were pelleted by centrifugation and resuspended in 100 μL of nuclei lysis buffer (50 mM Tris-HCl, 10 mM EDTA, 1% SDS). Next, samples were diluted 1:4.5 in dilution buffer (0.01% SDS, 1.1% Triton X-100, 1.2 mM EDTA, 16.7 mM Tris-HCl, 167 mM NaCl) and subjected to 15 cycles of sonication (for NT2 cells) or 30 cycles (for HeLa cells); each cycle included 30 sec of sonication and 30 sec of interval.

Sonicated chromatin was incubated overnight at 4°C with a 50% slurry of protein A–Sepharose beads blocked with yeast transfer RNA (Sigma, R8759) together with the appropriate antibody. Immunoprecipitates were washed with dilution buffer and eluted with 50 mM NaHCO$_3$, 1% SDS. DNase-free RNase and Proteinase K were added to the immunoprecipitated chromatin to final concentrations of 50 ng/mL and 200 ng/mL, respectively, followed by incubation for 3 h at 45°C. To complete reversal of crosslinks, samples were incubated overnight at 65°C. DNA was purified using the Qiagen PCR purification kit according to the manufacturer's protocol and analyzed by qPCR.

High-throughput sequencing was performed with Illumina Genome Analyzer IIx (GAIIx) sequencer on 20 ng of DNA from H2Bub1 and H2B ChIP.

Bioinformatic analyses

All ChIP-seq data were aligned to the hg18 human genome assembly using Bowtie (Langmead et al. 2009) while allowing for one mismatch per read, and only uniquely mapped reads were used for further processing. ChIP-seq peak enrichment and annotation analyses were carried out using HOMER (Heinz et al. 2010). All other analyses were carried out using a custom perl and R (R Development Core Team 2014) pipeline. Briefly, gene and exon annotations were derived from hg18 RefSeq gene annotations downloaded from the UCSC Genome Browser (Rhead et al. 2010). Single–base-pair resolution maps were constructed for each mapped ChIP-seq data set, cast upon the examined genomic segments in each analysis, and plotted with or without applying a moving average to smooth the signal, as specified throughout the text. When scaled to fit a set size, all examined genes or introns shorter than the set size were discarded. All sequences were aligned to the plus strand. NT2 and HCT116 gene expression data were derived from Fuchs et al. (2012) and Zhang et al. (2013), respectively. Genes were considered expressed if included in the two top bins of all gene expression levels of a given cell line divided into three equally sized bins. POLR2A ChIP-seq data in HCT116 generated with the 4H8 antibody was derived from http://genome.ucsc.edu/ENCODE/ (GSM803474) (The ENCODE Project Consortium 2012). Cluster 3.0 (http://bonsai. hgc.jp/~mdehoon/software/cluster/software.htm) and Java TreeView (Saldanha 2004) were used for the clustering and plotting of Supplemental Figure S1A. For the analysis presented in Figure 5B, peak calling was performed using N.Yoder peak finder (mathworks.com); only genes with at least one peak were selected.

Data access

The sequencing data from this study have been submitted to the NCBI Gene Expression Omnibus (GEO; http://www.ncbi.nlm.nih.gov/geo/) under accession number GSE56279.

Acknowledgments

References

Amit I, Citri A, Shay T, Lu Y, Katz M, Zhang F, Tarcic G, Siwak D, Lahad J, Jacob-Hirsch J, et al. 2007. A module of negative feedback regulators defines growth factor signaling. *Nat Genet* **39:** 503–512.

Barski A, Cuddapah S, Cui K, Roh TY, Schones DE, Wang Z, Wei G, Chepelev I, Zhao K. 2007. High-resolution profiling of histone methylations in the human genome. *Cell* **129:** 823–837.

Batta K, Zhang Z, Yen K, Goffman DB, Pugh BF. 2011. Genome-wide function of H2B ubiquitylation in promoter and genic regions. *Genes Dev* **25:** 2254–2265.

Berger SL. 2007. The complex language of chromatin regulation during transcription. *Nature* **447:** 407–412.

Blahnik KR, Dou L, Echipare L, Iyengar S, O'Geen H, Sanchez E, Zhao Y, Marra MA, Hirst M, Costello JF, et al. 2011. Characterization of the contradictory chromatin signatures at the 3′ exons of zinc finger genes. *PLoS ONE* **6:** e17121.

Blank M, Tang Y, Yamashita M, Burkett SS, Cheng SY, Zhang YE. 2012. A tumor suppressor function of Smurf2 associated with controlling chromatin landscape and genome stability through RNF20. *Nat Med* **18:** 227–234.

Braunschweig U, Gueroussov S, Plocik AM, Graveley BR, Blencowe BJ. 2013. Dynamic integration of splicing within gene regulatory pathways. *Cell* **152:** 1252–1269.

Briggs SD, Xiao T, Sun ZW, Caldwell JA, Shabanowitz J, Hunt DF, Allis CD, Strahl BD. 2002. Gene silencing: *trans*-histone regulatory pathway in chromatin. *Nature* **418:** 498.

Buszczak M, Paterno S, Spradling AC. 2009. *Drosophila* stem cells share a common requirement for the histone H2B ubiquitin protease scrawny. *Science* **323:** 248–251.

Campos EI, Reinberg D. 2009. Histones: annotating chromatin. *Annu Rev Genet* **43:** 559–599.

Chandrasekharan MB, Huang F, Sun ZW. 2009. Ubiquitination of histone H2B regulates chromatin dynamics by enhancing nucleosome stability. *Proc Natl Acad Sci* **106:** 16686–16691.

Chernikova SB, Dorth JA, Razorenova OV, Game JC, Brown JM. 2010. Deficiency in Bre1 impairs homologous recombination repair and cell cycle checkpoint response to radiation damage in mammalian cells. *Radiat Res* **174:** 558–565.

Davie JR, Murphy LC. 1990. Level of ubiquitinated histone H2B in chromatin is coupled to ongoing transcription. *Biochemistry* **29:** 4752–4757.

de Almeida SF, Grosso AR, Koch F, Fenouil R, Carvalho S, Andrade J, Levezinho H, Gut M, Eick D, Gut I, et al. 2011. Splicing enhances recruitment of methyltransferase HYPB/Setd2 and methylation of histone H3 Lys36. *Nat Struct Mol Biol* **18:** 977–983.

de la Mata M, Alonso CR, Kadener S, Fededa JP, Blaustein M, Pelisch F, Cramer P, Bentley D, Kornblihtt AR. 2003. A slow RNA polymerase II affects alternative splicing in vivo. *Mol Cell* **12:** 525–532.

Edmunds JW, Mahadevan LC, Clayton AL. 2008. Dynamic histone H3 methylation during gene induction: HYPB/Setd2 mediates all H3K36 trimethylation. *EMBO J* **27:** 406–420.

The ENCODE Project Consortium. 2012. An integrated encyclopedia of DNA elements in the human genome. *Nature* **489:** 57–74.

Fierz B, Chatterjee C, McGinty RK, Bar-Dagan M, Raleigh DP, Muir TW. 2011. Histone H2B ubiquitylation disrupts local and higher-order chromatin compaction. *Nat Chem Biol* **7:** 113–119.

Fleming AB, Kao CF, Hillyer C, Pikaart M, Osley MA. 2008. H2B ubiquitylation plays a role in nucleosome dynamics during transcription elongation. *Mol Cell* **31:** 57–66.

Fonseca GJ, Thillainadesan G, Yousef AF, Ablack JN, Mossman KL, Torchia J, Mymryk JS. 2012. Adenovirus evasion of interferon-mediated innate immunity by direct antagonism of a cellular histone posttranslational modification. *Cell Host Microbe* **11:** 597–606.

Fuchs G, Oren M. 2014. Writing and reading H2B monoubiquitylation. *Biochim Biophys Acta* **1839:** 694–701.

Fuchs G, Shema E, Vesterman R, Kotler E, Wolchinsky Z, Wilder S, Golomb L, Pribluda A, Zhang F, Haj-Yahya M, et al. 2012. RNF20

and USP44 regulate stem cell differentiation by modulating H2B monoubiquitylation. *Mol Cell* **46:** 662–673.

Fuchs G, Voichek Y, Benjamin S, Gilad S, Amit I, Oren M. 2014. 4sUDRB-seq: measuring genomewide transcriptional elongation rates and initiation frequencies within cells. *Genome Biol* **15:** R69.

Gelfman S, Burstein D, Penn O, Savchenko A, Amit M, Schwartz S, Pupko T, Ast G. 2012. Changes in exon-intron structure during vertebrate evolution affect the splicing pattern of exons. *Genome Res* **22:** 35–50.

Guttman M, Amit I, Garber M, French C, Lin MF, Feldser D, Huarte M, Zuk O, Carey BW, Cassady JP, et al. 2009. Chromatin signature reveals over a thousand highly conserved large non-coding RNAs in mammals. *Nature* **458:** 223–227.

Heinz S, Benner C, Spann N, Bertolino E, Lin YC, Laslo P, Cheng JX, Murre C, Singh H, Glass CK. 2010. Simple combinations of lineage-determining transcription factors prime *cis*-regulatory elements required for macrophage and B cell identities. *Mol Cell* **38:** 576–589.

Henry KW, Wyce A, Lo WS, Duggan LJ, Emre NC, Kao CF, Pillus L, Shilatifard A, Osley MA, Berger SL. 2003. Transcriptional activation via sequential histone H2B ubiquitylation and deubiquitylation, mediated by SAGA-associated Ubp8. *Genes Dev* **17:** 2648–2663.

Herissant L, Moehle EA, Bertaccini D, Van Dorsselaer A, Schaeffer-Reiss C, Guthrie C, Dargemont C. 2014. H2B ubiquitylation modulates spliceosome assembly and function in budding yeast. *Biol Cell* **106:** 126–138.

Huff JT, Plocik AM, Guthrie C, Yamamoto KR. 2010. Reciprocal intronic and exonic histone modification regions in humans. *Nat Struct Mol Biol* **17:** 1495–1499.

Hwang WW, Madhani HD. 2009. Nonredundant requirement for multiple histone modifications for the early anaphase release of the mitotic exit regulator Cdc14 from nucleolar chromatin. *PLoS Genet* **5:** e1000588.

Hwang WW, Venkatasubrahmanyam S, Ianculescu AG, Tong A, Boone C, Madhani HD. 2003. A conserved RING finger protein required for histone H2B monoubiquitination and cell size control. *Mol Cell* **11:** 261–266.

Ip JY, Schmidt D, Pan Q, Ramani AK, Fraser AG, Odom DT, Blencowe BJ. 2011. Global impact of RNA polymerase II elongation inhibition on alternative splicing regulation. *Genome Res* **21:** 390–401.

Johnsen SA. 2012. The enigmatic role of H2Bub1 in cancer. *FEBS Lett* **586:** 1592–1601.

Jonkers I, Kwak H, Lis JT. 2014. Genome-wide dynamics of Pol II elongation and its interplay with promoter proximal pausing, chromatin, and exons. *eLife* **3:** e02407.

Jung I, Kim SK, Kim M, Han YM, Kim YS, Kim D, Lee D. 2012. H2B monoubiquitylation is a 5′-enriched active transcription mark and correlates with exon-intron structure in human cells. *Genome Res* **22:** 1026–1035.

Kari V, Shchebet A, Neumann H, Johnsen SA. 2011. The H2B ubiquitin ligase RNF40 cooperates with SUPT16H to induce dynamic changes in chromatin structure during DNA double-strand break repair. *Cell Cycle* **10:** 3495–3504.

Karpiuk O, Najafova Z, Kramer F, Hennion M, Galonska C, Konig A, Snaidero N, Vogel T, Shchebet A, Begus-Nahrmann Y, et al. 2012. The histone H2B monoubiquitination regulatory pathway is required for differentiation of multipotent stem cells. *Mol Cell* **46:** 705–713.

Ke S, Shang S, Kalachikov SM, Morozova I, Yu L, Russo JJ, Ju J, Chasin LA. 2011. Quantitative evaluation of all hexamers as exonic splicing elements. *Genome Res* **21:** 1360–1374.

Kim J, Hake SB, Roeder RG. 2005. The human homolog of yeast BRE1 functions as a transcriptional coactivator through direct activator interactions. *Mol Cell* **20:** 759–770.

Kim J, Guermah M, McGinty RK, Lee JS, Tang Z, Milne TA, Shilatifard A, Muir TW, Roeder RG. 2009. RAD6-mediated transcription-coupled H2B ubiquitylation directly stimulates H3K4 methylation in human cells. *Cell* **137:** 459–471.

Kim S, Kim H, Fong N, Erickson B, Bentley DL. 2011. Pre-mRNA splicing is a determinant of histone H3K36 methylation. *Proc Natl Acad Sci* **108:** 13564–13569.

Kolasinska-Zwierz P, Down T, Latorre I, Liu T, Liu XS, Ahringer J. 2009. Differential chromatin marking of introns and expressed exons by H3K36me3. *Nat Genet* **41:** 376–381.

Kornblihtt AR, Schor IE, Allo M, Dujardin G, Petrillo E, Munoz MJ. 2013. Alternative splicing: a pivotal step between eukaryotic transcription and translation. *Nat Rev Mol Cell Biol* **14:** 153–165.

Kouzarides T. 2007. Chromatin modifications and their function. *Cell* **128:** 693–705.

Kwak H, Fuda NJ, Core LJ, Lis JT. 2013. Precise maps of RNA polymerase reveal how promoters direct initiation and pausing. *Science* **339:** 950–953.

Langmead B, Trapnell C, Pop M, Salzberg SL. 2009. Ultrafast and memory-efficient alignment of short DNA sequences to the human genome. *Genome Biol* **10:** R25.

Le Martelot G, Canella D, Symul L, Migliavacca E, Gilardi F, Liechti R, Martin O, Harshman K, Delorenzi M, Desvergne B, et al. 2012. Genome-wide RNA polymerase II profiles and RNA accumulation reveal kinetics of transcription and associated epigenetic changes during diurnal cycles. *PLoS Biol* **10:** e1001442.

Lee JS, Shukla A, Schneider J, Swanson SK, Washburn MP, Florens L, Bhaumik SR, Shilatifard A. 2007. Histone crosstalk between H2B monoubiquitination and H3 methylation mediated by COMPASS. *Cell* **131:** 1084–1096.

Llorian M, Schwartz S, Clark TA, Hollander D, Tan LY, Spellman R, Gordon A, Schweitzer AC, de la Grange P, Ast G, et al. 2010. Position-dependent alternative splicing activity revealed by global profiling of alternative splicing events regulated by PTB. *Nat Struct Mol Biol* **17:** 1114–1123.

Long L, Thelen JP, Furgason M, Haj-Yahya M, Brik A, Cheng D, Peng J, Yao T. 2014. The U4/U6 recycling factor SART3 has histone chaperone activity and associates with USP15 to regulate H2B deubiquitination. *J Biol Chem* **289:** 8916–8930.

Luco RF, Pan Q, Tominaga K, Blencowe BJ, Pereira-Smith OM, Misteli T. 2010. Regulation of alternative splicing by histone modifications. *Science* **327:** 996–1000.

Luco RF, Allo M, Schor IE, Kornblihtt AR, Misteli T. 2011. Epigenetics in alternative pre-mRNA splicing. *Cell* **144:** 16–26.

Maunakea AK, Chepelev I, Cui K, Zhao K. 2013. Intragenic DNA methylation modulates alternative splicing by recruiting MeCP2 to promote exon recognition. *Cell Res* **23:** 1256–1269.

Meshorer E, Yellajoshula D, George E, Scambler PJ, Brown DT, Misteli T. 2006. Hyperdynamic plasticity of chromatin proteins in pluripotent embryonic stem cells. *Dev Cell* **10:** 105–116.

Minsky N, Shema E, Field Y, Schuster M, Segal E, Oren M. 2008. Monoubiquitinated H2B is associated with the transcribed region of highly expressed genes in human cells. *Nat Cell Biol* **10:** 483–488.

Miyazaki H, Higashimoto K, Yada Y, Endo TA, Sharif J, Komori T, Matsuda M, Koseki Y, Nakayama M, Soejima H, et al. 2013. Ash1l methylates lys36 of histone h3 independently of transcriptional elongation to counteract polycomb silencing. *PLoS Genet* **9:** e1003897.

Moehle EA, Ryan CJ, Krogan NJ, Kress TL, Guthrie C. 2012. The yeast SR-like protein Npl3 links chromatin modification to mRNA processing. *PLoS Genet* **8:** e1003101.

Moyal L, Lerenthal Y, Gana-Weisz M, Mass G, So S, Wang SY, Eppink B, Chung YM, Shalev G, Shema E, et al. 2011. Requirement of ATM-dependent monoubiquitylation of histone H2B for timely repair of DNA double-strand breaks. *Mol Cell* **41:** 529–542.

Nakamura K, Kato A, Kobayashi J, Yanagihara H, Sakamoto S, Oliveira DV, Shimada M, Tauchi H, Suzuki H, Tashiro S, et al. 2011. Regulation of homologous recombination by RNF20-dependent H2B ubiquitination. *Mol Cell* **41:** 515–528.

Ng HH, Xu RM, Zhang Y, Struhl K. 2002. Ubiquitination of histone H2B by Rad6 is required for efficient Dot1-mediated methylation of histone H3 lysine 79. *J Biol Chem* **277:** 34655–34657.

Patel DJ, Wang Z. 2013. Readout of epigenetic modifications. *Annu Rev Biochem* **82:** 81–118.

Pavri R, Zhu B, Li G, Trojer P, Mandal S, Shilatifard A, Reinberg D. 2006. Histone H2B monoubiquitination functions cooperatively with FACT to regulate elongation by RNA polymerase II. *Cell* **125:** 703–717.

Pirngruber J, Shchebet A, Schreiber L, Shema E, Minsky N, Chapman RD, Eick D, Aylon Y, Oren M, Johnsen SA. 2009. CDK9 directs H2B monoubiquitination and controls replication-dependent histone mRNA 3′-end processing. *EMBO Rep* **10:** 894–900.

R Development Core Team. 2014 R: *a language and environment for statistical computing*. R Foundation for Statistical Computing, Vienna, Austria. http://www.R-project.org/.

Rhead B, Karolchik D, Kuhn RM, Hinrichs AS, Zweig AS, Fujita PA, Diekhans M, Smith KE, Rosenbloom KR, Raney BJ, et al. 2010. The UCSC Genome Browser database: update 2010. *Nucleic Acids Res* **38:** D613–D619.

Sadeghi L, Siggens L, Svensson JP, Ekwall K. 2014. Centromeric histone H2B monoubiquitination promotes noncoding transcription and chromatin integrity. *Nat Struct Mol Biol* **21:** 236–243.

Saldanha AJ. 2004. Java Treeview–extensible visualization of microarray data. *Bioinformatics* **20:** 3246–3248.

Sarkari F, Sanchez-Alcaraz T, Wang S, Holowaty MN, Sheng Y, Frappier L. 2009. EBNA1-mediated recruitment of a histone H2B deubiquitylating complex to the Epstein-Barr virus latent origin of DNA replication. *PLoS Pathog* **5:** e1000624.

Schor IE, Rascovan N, Pelisch F, Allo M, Kornblihtt AR. 2009. Neuronal cell depolarization induces intragenic chromatin modifications affecting NCAM alternative splicing. *Proc Natl Acad Sci* **106:** 4325–4330.

Schor IE, Fiszbein A, Petrillo E, Kornblihtt AR. 2013. Intragenic epigenetic changes modulate NCAM alternative splicing in neuronal differentiation. *EMBO J* **32:** 2264–2274.

Schwartz S, Meshorer E, Ast G. 2009. Chromatin organization marks exon-intron structure. *Nat Struct Mol Biol* **16:** 990–995.

Sen R, Bhaumik SR. 2013. Transcriptional stimulatory and repressive functions of histone H2B ubiquitin ligase. *Transcription* **4:** 221–226.

Shema E, Tirosh I, Aylon Y, Huang J, Ye C, Moskovits N, Raver-Shapira N, Minsky N, Pirngruber J, Tarcic G, et al. 2008. The histone H2B-specific ubiquitin ligase RNF20/hBRE1 acts as a putative tumor suppressor through selective regulation of gene expression. *Genes Dev* **22:** 2664–2676.

Shema-Yaacoby E, Nikolov M, Haj-Yahya M, Siman P, Allemand E, Yamaguchi Y, Muchardt C, Urlaub H, Brik A, Oren M, et al. 2013. Systematic identification of proteins binding to chromatin-embedded ubiquitylated H2B reveals recruitment of SWI/SNF to regulate transcription. *Cell Reports* **4:** 601–608.

Singh J, Padgett RA. 2009. Rates of in situ transcription and splicing in large human genes. *Nat Struct Mol Biol* **16:** 1128–1133.

Spies N, Nielsen CB, Padgett RA, Burge CB. 2009. Biased chromatin signatures around polyadenylation sites and exons. *Mol Cell* **36:** 245–254.

Sun ZW, Allis CD. 2002. Ubiquitination of histone H2B regulates H3 methylation and gene silencing in yeast. *Nature* **418:** 104–108.

Tilgner H, Nikolaou C, Althammer S, Sammeth M, Beato M, Valcarcel J, Guigo R. 2009. Nucleosome positioning as a determinant of exon recognition. *Nat Struct Mol Biol* **16:** 996–1001.

Trujillo KM, Osley MA. 2012. A role for H2B ubiquitylation in DNA replication. *Mol Cell* **48:** 734–746.

Veloso A, Kirkconnell KS, Magnuson B, Biewen B, Paulsen MT, Wilson TE, Ljungman M. 2014. Rate of elongation by RNA polymerase II is associated with specific gene features and epigenetic modifications. *Genome Res* **24:** 896–905.

Venkatesh S, Smolle M, Li H, Gogol MM, Saint M, Kumar S, Natarajan K, Workman JL. 2012. Set2 methylation of histone H3 lysine 36 suppresses histone exchange on transcribed genes. *Nature* **489:** 452–455.

Vitaliano-Prunier A, Babour A, Herissant L, Apponi L, Margaritis T, Holstege FC, Corbett AH, Gwizdek C, Dargemont C. 2012. H2B ubiquitylation controls the formation of export-competent mRNP. *Mol Cell* **45:** 132–139.

Wada Y, Ohta Y, Xu M, Tsutsumi S, Minami T, Inoue K, Komura D, Kitakami J, Oshida N, Papantonis A, et al. 2009. A wave of nascent transcription on activated human genes. *Proc Natl Acad Sci* **106:** 18357–18361.

Walter D, Matter A, Fahrenkrog B. 2010. Bre1p-mediated histone H2B ubiquitylation regulates apoptosis in *Saccharomyces cerevisiae*. *J Cell Sci* **123:** 1931–1939.

Wang Z, Zang C, Rosenfeld JA, Schones DE, Barski A, Cuddapah S, Cui K, Roh TY, Peng W, Zhang MQ, et al. 2008. Combinatorial patterns of histone acetylations and methylations in the human genome. *Nat Genet* **40:** 897–903.

Weake VM, Workman JL. 2008. Histone ubiquitination: triggering gene activity. *Mol Cell* **29:** 653–663.

Weinberger L, Voichek Y, Tirosh I, Hornung G, Amit I, Barkai N. 2012. Expression noise and acetylation profiles distinguish HDAC functions. *Mol Cell* **47:** 193–202.

Weiner A, Chen HV, Liu CL, Rahat A, Klien A, Soares L, Gudipati M, Pfeffner J, Regev A, Buratowski S, et al. 2012. Systematic dissection of roles for chromatin regulators in a yeast stress response. *PLoS Biol* **10:** e1001369.

Wood A, Krogan NJ, Dover J, Schneider J, Heidt J, Boateng MA, Dean K, Golshani A, Zhang Y, Greenblatt JF, et al. 2003. Bre1, an E3 ubiquitin ligase required for recruitment and substrate selection of Rad6 at a promoter. *Mol Cell* **11:** 267–274.

Wright DE, Wang CY, Kao CF. 2011. Flickin' the ubiquitin switch: the role of H2B ubiquitylation in development. *Epigenetics* **6:** 1165–1175.

Wu L, Zee BM, Wang Y, Garcia BA, Dou Y. 2011. The RING finger protein MSL2 in the MOF complex is an E3 ubiquitin ligase for H2B K34 and is involved in crosstalk with H3 K4 and K79 methylation. *Mol Cell* **43:** 132–144.

Yu P, Xiao S, Xin X, Song CX, Huang W, McDee D, Tanaka T, Wang T, He C, Zhong S. 2013. Spatiotemporal clustering of the epigenome reveals rules of dynamic gene regulation. *Genome Res* **23:** 352–364.

Zhang Z, Jones A, Joo HY, Zhou D, Cao Y, Chen S, Erdjument-Bromage H, Renfrow M, He H, Tempst P, et al. 2013. USP49 deubiquitinates histone H2B and regulates cotranscriptional pre-mRNA splicing. *Genes Dev* **27:** 1581–1595.

Zhou VW, Goren A, Bernstein BE. 2011. Charting histone modifications and the functional organization of mammalian genomes. *Nat Rev Genet* **12:** 7–18.

Zhu B, Zheng Y, Pham AD, Mandal SS, Erdjument-Bromage H, Tempst P, Reinberg D. 2005. Monoubiquitination of human histone H2B: the factors involved and their roles in HOX gene regulation. *Mol Cell* **20:** 601–611.